



Travel time after photobleaching velocimetry

Audrey J. Wang¹ · Jianyu Deng² · David Westbury² · Austin R. J. Downey^{2,3} · Yi Wang² · Guiren Wang^{2,4}

Received: 27 November 2023 / Revised: 11 March 2024 / Accepted: 27 March 2024 / Published online: 29 April 2024
© The Author(s) 2024

Abstract

In interfacial science and microfluidics, there is an increasing need for improving the ability to measure flow velocity profiles in the sub-micrometer range to better understand transport phenomena at interfaces, such as liquid–solid interfaces. Current standard methods of velocimetry typically use particles as tracers. However, seed particles can encounter issues at liquid and solid interfaces, where charge interactions between particles and surfaces can limit their ability to measure near-wall flows accurately. Furthermore, in many flows, seed particles have a different velocity from that of their surrounding fluid, which the particles are intended to represent. Several molecular tracer-based velocimeters have been developed which can bypass these issues. However, they either have limited resolution for measurement near solid surfaces, such as for slip flows, or require pre-calibration. Laser-induced fluorescence photobleaching anemometry (LIFPA) is one such technique that is noninvasive and has achieved unprecedented nanoscopic resolution for flow velocity profile measurement. However, it also requires pre-calibration, which is unavailable for unknown flows. Here, we present a novel, calibration-free technique called travel time after photobleaching (TTAP) velocimetry, which can measure flow velocity profiles and near-wall flow with high spatiotemporal resolution. Furthermore, TTAP velocimetry is compatible with LIFPA, and thus, the two systems can be coupled to satisfy LIFPA's long-anticipated need for pre-calibration, enabling measurement of flow velocity profiles in unknown flows with salient resolution.

1 Introduction

In interfacial science, the ability to measure flow velocity profiles with nanoscopic resolution is critical to understanding transport phenomena at interfaces in many flows. These include, but are not limited to, flows in micro- and nanofluidics, AC electrokinetics, electric double layers, blood capillaries, non-Newtonian flows, and flows in porous media. The development of a technique that meets the urgent need for ultrahigh spatial and temporal resolution has been a

major effort in fluid dynamics and could deepen our current understanding of flows and transport at interfaces. Such a technique could help determine whether a flow has a slip or no-slip boundary condition over a solid surface, a topic that has been heavily debated over the past two centuries with no definitive conclusion (Neto et al. 2005; Sochi 2011; Vinogradova et al. 2009). In fact, recently, there has been a growing interest in the effects of hydrophobicity on fluid–solid interactions (Ho et al. 2011; Rothstein 2010; Schäffel et al. 2016; Schmitz et al. 2011; Xu et al. 2021), where slip length is shown to be correlated with drag reduction (Rothstein 2010; Schmitz et al. 2011, Xu et al. 2021). Such a technique could also help to elucidate biological processes of mechanotransduction, where it has been realized that fluid shear stress plays an important role in physiology and pathology (Freund and Vermot 2014; Urschel et al. 2021). The ability to measure velocity profiles on the sub-micrometer scale could also enable study of flows in porous media, which are presently still poorly understood. This includes flows in human tissues, oil shale, and soil, among others, with important applications in microvasculature transport, groundwater pollution, geological storage of carbon dioxide, and battery design (Aminpour et al. 2018; Puyguiraud et al. 2021).

✉ Yi Wang
yiwang@cec.sc.edu

✉ Guiren Wang
guirenwang@sc.edu

¹ Department of Chemistry and Biochemistry, University of South Carolina, Columbia, SC 29208, USA

² Department of Mechanical Engineering, University of South Carolina, Columbia, SC 29208, USA

³ Department of Civil and Environmental Engineering, University of South Carolina, Columbia, SC 29208, USA

⁴ Department of Biomedical Engineering, University of South Carolina, Columbia, SC 29208, USA

Here, the hydraulic diameter of pores can range from a few micrometers down to tens of nanometers.

Current standard techniques to measure flows primarily rely on particles as tracers. Some examples include the widely known micro- and nanoparticle image velocimetry (μ PIV Santiago et al. 1998; Wereley and Meinhart 2010) and nPIV (Jin et al. 2004; Zettner et al. 2003)) and laser Doppler velocimetry (Aksel and Schmidtchen 1996). Although instrumental to advancing flow measurement, these methods have their own challenges. While seed particles have been assumed to reliably represent their surrounding fluids, this is often not the case. In fact, in many microflows, particles do not have the same velocity as their surrounding fluids, such as in electrokinetics, magnetophoresis, acoustophoresis, photophoresis, thermophoresis, and near-wall flows (Lauga et al. 2007; Zhao et al. 2016). Complications can arise from error due to electrostatic interactions between the surface and the seed particles (Lauga et al. 2007). If the two are similarly charged, electrostatic repulsion will prevent the particles from entering a certain distance from the wall, which can affect reliable measurement of near-wall flows. Particle-based methods also suffer from resolution limits, which make it difficult to accurately measure slip flows. This is because the best resolution achieved thus far through PIV is on the similar order of—or even larger than—the measured slip length (Rothstein 2010; Schmitz et al. 2011). If the size of the resolution is larger than the slip length, then, it is impossible to directly measure the slip length accurately. Furthermore, most measured slip lengths are shorter than 100 nm, yet almost all optics-based methods used today suffer from the diffraction limit of roughly 200 nm (Gryczynski 2008; Huang et al. 2009), limiting the spatial resolution of particle-based methods.

The use of neutral molecular dye as a tracer bypasses these issues of using particles as tracers. The small size and electrical properties of certain dyes make them ideal tracers for fluid flow since the dye moves at the same speed as its surrounding fluid and does not interact electrically with the solid wall or other molecules, unlike larger particles. However, current methods tend to suffer from limited temporal and spatial resolution (also due to the diffraction limit), such as molecular tagging velocimetry (Hu and Koochesfahani 2006) and fluorescence photobleaching recovery (Flamion et al. 1991). A recent method has been developed that uses periodic photobleaching of dyed fluid to measure bulk average flow by evaluating the time of migration of a photobleached blot in the flow (Pittman et al. 2003). This method requires two lenses, one for photobleaching the dye and the other for measuring the fluorescence signal. Thus, it also requires pre-calibration to estimate the distance between the two laser foci and has limited resolution that can only measure bulk flow velocity. Additionally, the use of two lenses severely limits this

method from being compatible with a microscope, which has only one objective.

Laser-induced fluorescence photobleaching anemometry (LIFPA) (Wang 2005; Zhao et al. 2016) is a method which uses small, neutral molecular dye as a flow tracer to measure flow velocities according to fluorescence intensity with both high temporal and spatial resolution. LIFPA can be thought of as a noninvasive, optical counterpart of hot-wire anemometry, which utilizes a wire analogous to the beam used in LIFPA, and both require calibration between flow velocity and voltage (Kim and Fiedler 1989). As a result of its ultrahigh-resolution, LIFPA has recently led to several new discoveries, such as measurement of electrokinetic turbulence and chaotic flow in microfluidics (Hu et al. 2020; Wang et al. 2014; Zhao et al. 2018). LIFPA's functionality is further enhanced by its compatibility with the revolutionary technology of stimulated emission depletion (STED) (Hell 2007) in a method referred to as STED-LIFPA. The integrated STED technology enables LIFPA to bypass the light diffraction limit to achieve a spatial resolution of 70 nm (Kuang and Wang 2010). As Cuenca et al. mentioned (Cuenca and Bodiguel 2012), STED-LIFPA is the only method thus far that is able to acquire three-dimensional velocity profiles below the microscale. While its resolution can enable near-wall flow measurements, LIFPA can also be used for velocity measurement in macroflows (Wang and Fiedler 2000). Despite this achievement, as pointed out by Schembri et al. (Schembri et al. 2015), the main challenge of this method lies in its need for calibration of fluorescence intensity prior to velocity measurements, which is not available for unknown flows. This raises the need for a calibration-free velocimeter that can be made compatible with LIFPA's setup to help calibrate LIFPA and STED-LIFPA.

To address this need, we present a calibration-free single point method called travel time after photobleaching (TTAP) velocimetry that can measure flow velocity profiles in a capillary with high spatial resolution up to the light diffraction limit. It uses small, neutral molecular dye as a tracer, which can faithfully follow its surrounding fluid, and is compatible with a microscope for ease of use. Additionally, our setup shares the same optical setup with LIFPA, making it readily available for LIFPA calibration at any time if needed. It is also compatible with STED-LIFPA for potential nanosocopic measurements in the future.

2 Principle of TTAP velocimetry

Just as LIFPA is analogous to hot-wire anemometry, TTAP velocimetry is analogous to hot-wire anemometry with multiple parallel wires, but noninvasive and with high resolution (Kim and Fiedler 1989). The proposed method is illustrated

in Fig. 1a. Two laser foci are required, which can be achieved using either two lasers (as in the present work) or one laser with a beam splitter. Both lasers focus within a flow field (capillary used in the present work), through which a fluid containing a small, neutral molecular dye flows. In 1D flow measurements, the two laser foci are aligned to the same y - and z -positions at the capillary, but different streamwise x -positions. The distance between the streamwise foci is the travel distance length L .

The first laser, referred to as the photobleaching laser, or laser P in Fig. 1a, is positioned at position P' in the capillary. The photobleaching laser is periodically pulsed with a given pulse width t_{pw} and frequency f_p to generate a photobleached blot of dye in the moving fluid. A portion of this laser light is directed toward a photon detector, allowing pulses to be identified as peaks in a time series of light intensity, indicating the photobleaching start time. The second laser, referred to as the detection laser, or laser D, is a continuous wave (cw) laser that focuses downstream at position D'. Fluid inside the capillary flows from position P' to D', and the distance between these positions is equal to L . The detection laser is a probe laser that continuously induces fluorescence in the moving dye inside the capillary. The fluorescence intensity I_f at

the focus of the detection laser is measured by the same detector that measures the photobleaching pulses. When a blot of bleached dye reaches position D', a dip in I_f is observed.

In the final time series of light intensity, as shown in Fig. 1b, the time measured from a peak to its corresponding dip indicates the travel time t_t , or the time it takes for the dye to travel a distance of L . If the distance L between positions P' and D' can be directly measured by a camera, then, the flow velocity v can be determined by the following:

$$v = \frac{L}{t_t} \tag{1}$$

Since this method has a microscale L and sub-nanoscale laser focus, Taylor dispersion has a negligible effect on the blot's deformation.

Several important aspects must be considered for high resolution measurement. First, although two laser beams are required for their respective functions, both must pass through one objective to be fully compatible with a microscope and to measure L accurately. To do this, rather than having the lasers enter the pupil of the objective parallel to each other, they should enter at an angle. This can be adjusted by tuning mirror 2 shown in Fig. 1a, which changes the angle of the photobleaching laser beam. This allows the detection laser to enter the pupil parallel to the axis of the objective, while the photobleaching laser enters at an adjustable angle. By maintaining the alignment of the detection laser with the axis of the objective, this technique becomes compatible with LIFPA. The angled entrance of the two lasers through one objective also allows for a sufficiently small L , which can minimize velocity measurement complications caused by fluorescence recovery due to molecular diffusion at the bleached blot of dye. Since fluorescence recovery increases with increasing t_t , the dip in fluorescence signal becomes less pronounced at low velocities. Therefore, L should be adjustable to enable measurement of a large dynamic range of velocities. Finally, to ensure that this method is indeed calibration-free, L should be directly measurable. This is made possible through the use of one objective rather than two. To measure L , a stage micrometer (not shown here) is placed at the focal point of the objective, and the distance between the two laser foci is measured on the micrometer using a camera. L can also be measured directly from an image of the capillary if the inner and outer capillary diameters are known, and the capillary walls and laser foci are visible, such as in Fig. 1c. This is done by comparing the pixel distance between the capillary walls with the known capillary outer diameter and using this scale to measure the pixel distance between the two laser foci.

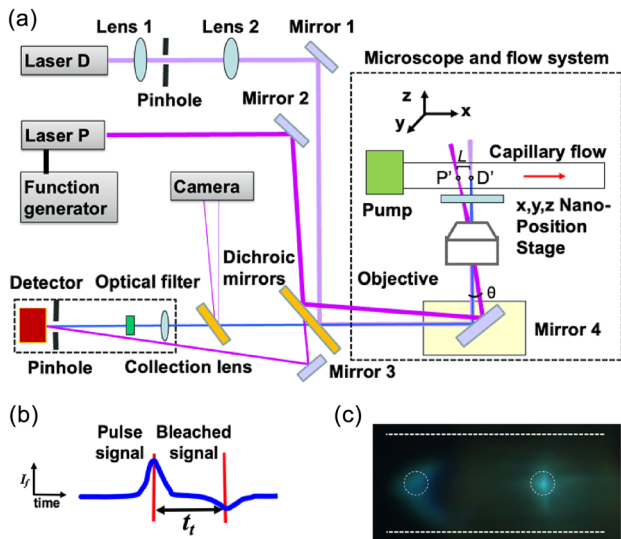


Fig. 1 Optical and flow system setup for TTAP velocimetry. **a** Schematic of the optical and flow system, showing path of laser beam D (lavender), P (fuchsia), and fluorescence signal (blue). **b** Time series of I_f showing a peak, which represents the pulse signal and start time of photobleaching, and a dip, which represents the time at which the photobleached blot of fluid passes through the detection beam. The difference in time between the peak and valley represents the t_t . **c** Image of the two laser foci at the capillary taken with a camera, with a distance L of 69 μm . The laser focused on the left is the photobleaching laser, and the one on the right is the detection laser. White dashed lines on the top and bottom represent capillary walls (inner diameter 50 μm)

An image from the camera used to measure the distance L within the capillary in the present study is shown in Fig. 1c.

3 Experimental setup

A schematic of the newly developed TTAP velocimeter is illustrated in Fig. 1a. Two laser diodes of wavelength 405 nm were used, a photobleaching laser (laser P) and a detection laser (laser D). The photobleaching laser (250 mW) was a pulsed laser used to generate photobleaching, and the detection laser (7 mW) was a cw laser used to induce fluorescence signal I_f in the moving dye through the capillary. A function generator (Tektronix AFG3102) was applied to the photobleaching laser to generate the pulses, allowing for adjustable pulse width t_{pw} and frequency f_p , which were modified based on velocity; at higher velocities, t_{pw} was decreased and f_p was increased, and vice versa.

To achieve the smallest laser focus diameter possible for high spatial resolution, the detection laser passed through a beam expander. Both lasers were reflected off a dichroic mirror before entering the camera port of a confocal microscope (Nikon C2). The portion of the photobleaching laser that passed through the dichroic mirror was redirected to a single photon detector (ID100-MMF50 from Photonic Solutions Ltd) with a mirror to monitor periodic photobleaching peaks in I_f time series. The detection laser was directed into the microscope's objective (oil immersion, 60 \times , numerical aperture (NA)/1.4) at an incident angle of 0 degrees, whereas the photobleaching laser entered at an angle θ . This enabled a tunable travel distance length L between the laser foci at the same y - and z -positions in the capillary by adjusting θ with mirror 2. L was measured using an image of the two laser foci within the capillary of known outer diameter taken with a camera. L can alternatively be measured using a stage micrometer placed at the focal point of the objective in place of the capillary. In the current work, L was set to a fixed distance of 69 μm . Figure 1c shows the two laser foci within the capillary.

The fluorescence I_f induced by the detection laser at the capillary was collected by the microscope's objective and passed through the dichroic mirror. The signal was then passed through a collection lens, an optical band filter, and a multimode fiber with a core diameter of 10 μm . Finally, the signal was detected by the same detector measuring the pulse signal and recorded onto the hard drive of a computer through an A/D converter (NI USB-6259). The signal was monitored and recorded using LabVIEW. The spatial resolution of our system was dependent on both the diameter of the detection laser at the objective's focal point and the fiber diameter at the detector and was estimated to be about 203 nm in the lateral direction based on the diffraction

limit, and about 610 nm in the axial direction. As TTAP scans laterally, rather than axially or vertically, the lateral resolution is more relevant in this system.

The present TTAP method was evaluated using pressure-driven laminar flows through a quartz capillary (inner diameter 50 μm , length 100 mm) driven by a syringe pump (Harvard 11 Pico Plus Elite) through a 10 μL glass syringe (Hamilton). All measurements were performed 50 mm downstream from the entrance of the capillary. Here, fluid flowed in the direction from position P' to D'. All velocity measurements were taken at the centerline (axis), except for the velocity profile measurement. We used Coumarin 102 (Santa Cruz Biotechnology, Inc) dissolved in water at a concentration of 100 μM as a tracer. The capillary was held in place by an XYZ piezo stage (P-545.3C7 PInano@ Cap XYZ Piezo Stage from Physik Instrumente), which has a resolution of 1 nm and was mounted on the confocal microscope. Time series scans of I_f were performed and recorded using PIMikroMove and LabVIEW, and data were processed using MATLAB.

4 Experimental results

The time series of I_f measured over time for three different centerline velocities u_c is shown in Fig. 2. These time series are a sum of I_f induced by the detection laser and light intensity from laser P's pulse, where the peaks represent each pulse of the photobleaching laser, and the valleys represent the dip in I_f when the bleached blot passes through the focus of the detection laser. The time between the peak and the valley represents the time of travel t_t across the distance L .

The time series in Fig. 2 show that when u_c was 0.14 mm/s, 1.42 mm/s, and 28.31 mm/s, the corresponding t_t was 0.5 s, 0.06 s, and 0.002 s, respectively. These results demonstrate that t_t decreased as u_c increased, as expected from the parabolic velocity profile of laminar flows in tubes, which confirms that the present TTAP technique can reliably measure flow velocity. Note the three centerline velocities show three orders of difference to demonstrate the large dynamic range. Additional centerline velocities within this range will show a similar trend.

Because t_t decreased as velocity increased, the sampling rate f_s was also increased with increasing velocity to ensure that t_t could still be detected. For the highest velocity, 28.31 mm/s, shown in Fig. 2c, the vertical lines representing the peak and valley are nearly indistinguishable in the time series due to the small t_t and zoomed-out x -axis for visual comparison to other velocities. Notice also that in lower velocities, there was a broadening in width of the valley, as its lower velocity allowed more time for molecular diffusion at the bleached blot. This change in valley width ΔW can be approximately explained by

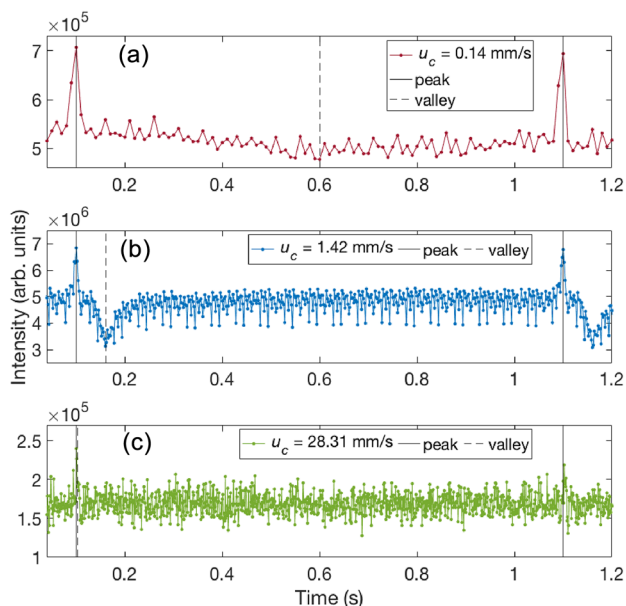


Fig. 2 Time series comparison of different centerline velocities and their respective measured travel times. The black solid line, or peak, represents the time of photobleaching, and the black dashed line, or valley, represents the time when the bleached blot reached the detection laser. The time difference between the peak and valley is equal to t_t . The pulse frequency was set to 1 Hz for each of these velocity measurements. **a** u_c of 0.14 mm/s with t_{pw} of 30 ms and f_s of 100 samples per second. **b** u_c of 1.42 mm/s with t_{pw} of 30 ms and f_s of 500 samples per second. **c** u_c of 28.31 mm/s with t_{pw} of 20 ms and f_s of 1000 samples per second

$$\Delta W \sim \sqrt{\frac{t_t}{D}} \tag{2}$$

where D is the diffusivity of the dye.

The proposed TTAP method shows great potential for measuring velocity over a large dynamic range. Figure 3 illustrates the dynamic range, which was determined by the maximum and minimum velocities that can be measured using TTAP with a fixed L . In capillary flows, there is a positive linear relationship between flow rate Q and centerline velocity u_c , which is observed in Fig. 3. Here, we demonstrate that u_c measured using TTAP aligns well with theoretical u_c (calculated as two times the theoretical bulk velocity). u_c was measured at various Q for a final measured velocity range of 0.028–28 mm/s, yielding a dynamic range of approximately 1000, or three orders of magnitude. The larger error associated with higher flow rates can be explained by the temporal resolution of our current system, which limited the ability to accurately detect high velocity signals. This error can be reduced by increasing the sampling rate of data collection. While lower velocities were measured, the percent error was found to be higher due to inconsistencies in the syringe pump’s performance at low flow rates ($Q < 0.1 \mu\text{L/hr}$).

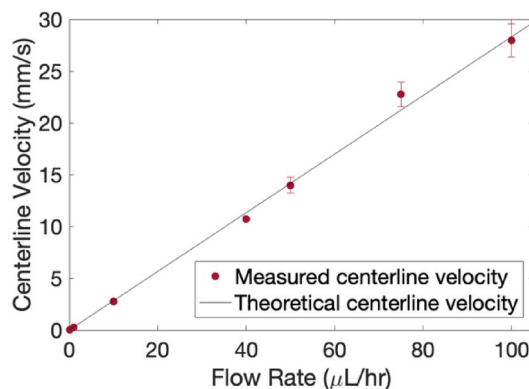


Fig. 3 Dynamic range showing maximum and minimum velocities that can be measured with TTAP with a fixed L (69 μm). Velocities were measured for a set of flow rates ranging from 0.1 to 100 $\mu\text{L/hr}$ for a final velocity range of 0.028–28 mm/s. Measured data includes error bars with ± 1 SD

The dynamic range can be increased by adjusting L or the objective magnification. For example, for measurement of higher velocities, one can increase L or decrease the objective magnification. Selection of the photobleaching pulse width t_{pw} and sampling rate f_s also depends on the velocity being measured. Higher velocities may need a shorter t_{pw} and higher f_s to ensure that the dynamic process can be distinguished and measured.

This technique can measure velocity with high temporal resolution, which is revealed in Fig. 4. Temporal resolution is determined by the smallest measurable length of t_t . Figure 4 shows a time series of I_f for a relatively high u_c of 28.3 mm/s and demonstrates that this method has a temporal resolution of 10 ms, as it can acquire travel time data every 10 ms. Furthermore, since t_t shown in this figure is less than $\frac{1}{2}$ of the time between each pulse, this suggests that our

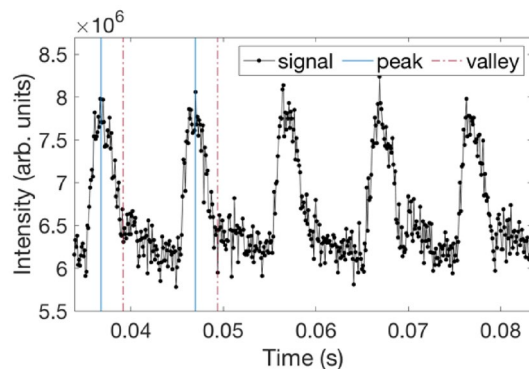


Fig. 4 Temporal resolution demonstrating the smallest measurable length of t_t . This I_f data for a velocity of 28.3 mm/s was measured with t_{pw} of 1.2 ms, f_p of 100 Hz, and f_s of 10,000 samples per second

method has the potential to achieve a temporal resolution of 5 ms.

Unlike Fig. 2, the lowest I_f values for each pulse shown in Fig. 4 do not represent the time point where the bleached blot reaches the detection laser; rather, there is a dip in the signal that can be seen before the lowest intensity values. The dip immediately follows the peak and represents the real t_t of the blot, indicated as the “valley” in this figure. This inference is based on the following: (1) this measured t_t is consistent with the theoretical t_t for this velocity; (2) this valley signal is repeatable; and (3) there is no such repeatable valley seen in lower u_c . This is likely due to the additional rise and fall time of the photobleaching laser’s pulse, which causes the photobleaching signal’s fall time to extend past the t_t signal at sufficiently high velocities. The current laser’s fall time was measured to be about 2 ms. Thus, to ensure that this method is calibration-free at high velocities, a pulse laser with sufficiently short rise and fall times should be used, so that its total pulse width does not interfere with t_t signal.

TTAP was also evaluated to measure the velocity profile of pressure-driven laminar flow through the capillary, which is theoretically parabolic. Figure 5 illustrates both the theoretical and average measured velocity profile of flow (10 $\mu\text{L/hr}$) in the capillary. This profile was formed by scanning the capillary with 1 μm steps across its diameter and measuring t_t at each radial position. The measured t_t were then used to calculate the velocity at each position with the same L . Figure 5 shows that the measured velocities closely resemble predicted values of Poiseuille flow. Based on the similarity of these profiles, it is clear that TTAP can measure the velocity profile of flow in a capillary.

It is interesting to note that in the measured velocity profile, the velocities near the wall ceased to follow the theoretical profile starting at approximately 4 μm away from

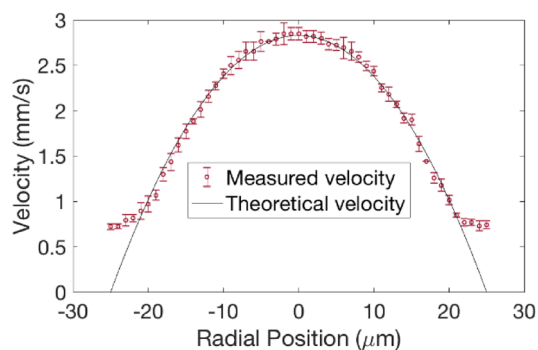


Fig. 5 Velocity profile of fluid flowing at a rate of 10 $\mu\text{L/hr}$ through a capillary with inner diameter of 50 μm . Lateral scans were performed with 1 μm steps in the radial direction with t_{pw} of 25 ms, f_p of 1 Hz, and f_s of 1000 samples per second. Measured data includes error bars with ± 1 SD

the wall. Rather, the velocities in the near-wall region began to level out at a nonzero value.

The reasoning behind these results is not entirely clear. We noticed that similar velocity profiles near the wall have been reported previously (Joseph and Tabeling 2005; Lumma et al. 2003), which are similar to ours and are not zero. Joseph and Tabling attributed the deviation from zero at wall to slip flow (Joseph and Tabeling 2005). Another explanation could be similar to that observed by Lumma et al., where the laser beam has a tail in its Gaussians distribution (Lumma et al. 2003). Although the center of the laser beam is out of the solid wall, the tail could still be within the flow field and cause the measured nonzero velocity near the wall. Here, we find that the higher the laser power, the larger the diameter of the tail of the Gaussians beam. The large tail could cause the error that velocity is larger than zero even through the center of the laser focus is on the wall. In the future, we can use a smaller pinhole to “see” and measure the velocity close to the wall within 4 μm . Other well-known reasons for apparent slip length and overestimation of velocity related to particle tracers, such as particle depletion, are not relevant to our system, since TTAP velocimetry is based on small molecular dye smaller than 1 nm in diameter. Total internal reflection could be another reason at the near-wall region when a large NA objective is used (Kuang et al. 2009). Further study is needed to fully explain this observation.

5 Discussion

5.1 TTAP resolution and maximum measurable velocity

In general, the temporal resolution of this method depends on several parameters, such as sampling rate, rise and fall times of the detector and each component used in the detection system, and in particular, laser pulse width and power, and the travel time of the present TTAP velocimetry. Specifically, the sampling rate of the detector should be sufficiently fast to record the signal events in a time series, and the system’s rise and fall times should be sufficiently small so as not to miss the real signal. For a given setup, if these conditions are assumed to be true and all noted parameters are fixed, then, the maximum velocity that can be tracked by TTAP velocimetry depends on the travel time t_t that can be distinguished. The smallest t_t that can be measured corresponds to the maximum velocity that can be measured. In other words, the smaller the detectable travel time t_t , the higher the velocity that can be measured. In Fig. 4, for the present setup, since L is short and the pulse width is relatively large (for a cw laser used here) when velocity is higher than 60 mm/s, the travel time t_t is

almost the same as the laser pulse width, and therefore, is not distinguishable. For accuracy, the maximum velocity shown here is 28 mm/s to demonstrate the concept and feasibility of TTAP velocimetry. With today’s advancements in semiconductors, the sampling rate and rise/fall times are generally not limiting factors for most single point measurements in fluid mechanics. There is still room and potential for improvement of the temporal resolution to increase the maximum measurable velocity and temporal resolution (e.g., by increasing L , reducing the laser pulse width, and increasing laser power).

The spatial resolution is normally determined by the smallest position size at which the velocity difference from its neighboring position can be distinguished. The present development of TTAP velocimetry is based on a conventional confocal microscope principle. The spatial resolution of a conventional confocal microscope is well-known to be diffraction limited. The diffraction limit can be bypassed through the revolutionary technology stimulated emission depletion (STED) used in LIFPA, which is compatible with TTAP velocimetry (Hell 2007; Kuang and Wang 2010).

5.2 Consideration of light refraction through the capillary

The distance L can be measured through direct imaging of the capillary or by using a micrometer, as explained in the experimental setup. Due to light refraction through the capillary, however, L measurements using a micrometer may need to be corrected to consider the changing refractive indices of the capillary, fluid, and surrounding media. This is because when light with an angle passes through media with different refractive indices, L in the flow channels could be different from that measured with a micrometer. For the setup described in this paper, the difference in L can be considered negligible ($< 3\%$). However, this may be important if direct imaging of the laser foci inside the capillary is not feasible, such as measurement through a blood vessel capillary or when the objective is not an oil or water immersion one. Figure 6 illustrates the refraction of light as it passes through a medium downstream from the lens, capillary, and fluid within the capillary.

To address this potential concern, we have included a model, which calculates the actual distance between foci within a capillary, $L_{capillary}$ or L_C , given the distance measured with a micrometer, $L_{micrometer}$ or L_M , the capillary’s dimensions, the objective’s working distance, and the refractive indices of the capillary, fluid inside the capillary, and the medium between the objective and the capillary.

To calculate the actual distance L_C between the two laser foci using a distance L_M measured with a micrometer, the working distance of the microscope objective can be used

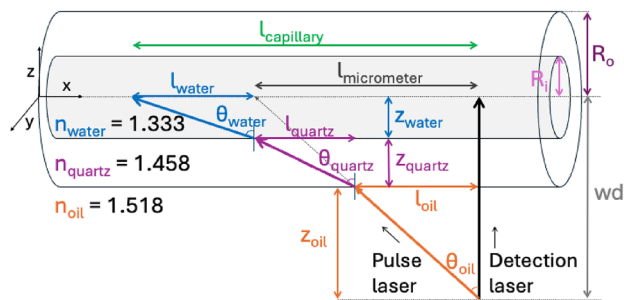


Fig. 6 Illustration of light refraction through capillary

to calculate the incident angle of the pulse laser through the oil with the following equation,

$$\tan\theta_{oil} = \frac{L_M}{wd} \tag{3}$$

where θ_{oil} is the incident angle of the pulse laser through the oil, and wd is the working distance of the objective.

Once θ_{oil} is known, based on Snell’s law, the incident angles of light through the quartz and water (i.e., the fluid within the capillary) can also be calculated using the following equations,

$$n_{oil}\sin\theta_{oil} = n_{quartz}\sin\theta_{quartz} = n_{water}\sin\theta_{water} \tag{4}$$

where n_{oil} , n_{quartz} , and n_{water} are the refractive indices of each medium, and θ_{quartz} and θ_{water} are the incident angles through quartz and water, respectively.

The capillary dimensions can be used to calculate the height in the z -direction that light travels through each medium, we then have

$$z_{oil} = wd - R_o \tag{5}$$

$$z_{quartz} = R_o - R_i \tag{6}$$

$$z_{water} = R_i \tag{7}$$

where R_o is the capillary’s outer radius, R_i is the inner radius, and z is the height at which light passes through each medium.

With the incident angle and height at which light passes through each medium known, the axial distance light travels through each medium can be calculated using simple trigonometry,

$$l_{oil} = z_{oil}\tan\theta_{oil} \tag{8}$$

$$l_{quartz} = z_{quartz}\tan\theta_{quartz} \tag{9}$$

$$l_{\text{water}} = z_{\text{water}} \tan \theta_{\text{water}} \quad (10)$$

where l is the distance along the capillary in the x -direction that light travels through each medium.

Finally, the total distance L_C between the laser foci at the centerline of the capillary can be calculated as the sum of distances through each medium,

$$L_C = l_{\text{oil}} + l_{\text{quartz}} + l_{\text{water}} \quad (11)$$

where L_C is the actual distance L between the two laser foci inside the capillary.

5.3 Applications

Since this is an initial effort of developing a new velocimetry method, experiments using one fluid operating at the Poiseuille flow regime were performed to prove the method's feasibility, reliability, and accuracy. This small molecular tracer-based method could be used for other transparent single-phase fluids (both Newtonian and non-Newtonian fluids) under the same principle. Since this is a calibration-free method based on molecular photobleaching, TTAP velocimetry is expected to be applicable to many other flows when combined with LIFPA. To establish feasibility, this new method was validated using an aqueous solution in the present work, while extensive demonstration for various samples of different properties and flows will be pursued in the future work. The current TTAP implementation is still subjected to the diffraction limit and has difficulty capturing the velocity profile near the wall but is expected to yield higher resolution when combined with STED-LIFPA. Since the method has demonstrated three-order dynamic range, which is sufficient for capturing velocity profiles in most applications, TTAP is expected to be applicable for measuring other velocity profiles in addition to the Poiseuille flow. In conjunction with LIFPA, which has more advanced capabilities, this system also enables study of more advanced flows, such as wall influence on flows, unsteady flows, and inertial particle focusing.

6 Conclusion

In conclusion, we have developed a new, single point velocimeter called travel time after photobleaching velocimetry that directly measures fluid flow velocity. This molecular tracer-based method bypasses issues with using particles as tracers and does not require pre-calibration. Furthermore, this method yields high spatial resolution estimated up to the diffraction limit, and its high temporal resolution and adjustable travel distance allow it to measure

a large dynamic range of velocities. In addition to being compatible with a microscope for ease of use, TTAP velocimetry has further been developed to be compatible with LIFPA, for which it can be used as calibration, raising the potential to achieve a new velocimetry system with ultrahigh spatiotemporal resolution.

While the current development is still limited by the diffraction limit, it has the potential to be integrated with STED-LIFPA, which could greatly enhance the resolution to pass the diffraction limit. Each of these techniques share similar optical setups that can precisely define the exact position of velocity measurements, especially in the near-wall region, holding great promise for slip flow and other interfacial flow measurements. Both TTAP and LIFPA can be used not only for flows at liquid and solid interfaces, micro- and nanofluidics, but also macro- and microflows. Ultimately, this new system could offer new nanoscopic velocimetry and change the paradigm of flow velocity profile measurement for studies of transport phenomena in interfacial science.

Acknowledgements We thank Akrm Abdalrahman for his help in preparing the flow setup and Alexander Vereen for his technical support.

Author contributions AW was involved in experiments, data processing, software, and main manuscript writing. JD contributed to software and manuscript reviewing. DW and AD contributed to experiments and manuscript reviewing. YW helped in supervising the project and manuscript preparation and editing. GW led the project and contributed to conceptualization, supervising, and manuscript preparation and editing.

Funding Open access funding provided by the Carolinas Consortium. This work was supported by the National Science Foundation under Grant No. CAREER CBET 0954977 and MRI CBET-1040227.

Declarations

Conflict of interest The authors declare that they have no conflicts of interest.

Data availability Data will be made available upon request.

Open Access This article is licensed under a Creative Commons Attribution 4.0 International License, which permits use, sharing, adaptation, distribution and reproduction in any medium or format, as long as you give appropriate credit to the original author(s) and the source, provide a link to the Creative Commons licence, and indicate if changes were made. The images or other third party material in this article are included in the article's Creative Commons licence, unless indicated otherwise in a credit line to the material. If material is not included in the article's Creative Commons licence and your intended use is not permitted by statutory regulation or exceeds the permitted use, you will need to obtain permission directly from the copyright holder. To view a copy of this licence, visit <http://creativecommons.org/licenses/by/4.0/>.

References

- Abarbanell AM, Herrmann JL, Weil BR et al (2010) Animal models of myocardial and vascular injury. *J Surg Res* 162:239–249. <https://doi.org/10.1016/j.jss.2009.06.021>
- Aksel N, Schmidtchen M (1996) Analysis of the overall accuracy in LDV measurement of film flow in an inclined channel. *Meas Sci Technol* 7:1140–1147
- Aminpour M, Galindo-Torres SA, Scheuermann A, Li L (2018) Slip-flow lattice-Boltzmann simulations in ducts and porous media: a full rehabilitation of spurious velocities. *Phys Rev E* 98:043110. <https://doi.org/10.1103/PhysRevE.98.043110>
- Cuenca A, Bodiguel H (2012) Fluorescence photobleaching to evaluate flow velocity and hydrodynamic dispersion in nanoslits. *Lab Chip* 12:1672–1679
- Flamion B, Bungay PM, Gibson CC, Spring KR (1991) Flow rate measurements in isolated perfused kidney tubules by fluorescence photobleaching recovery. *Biophys J* 60:1229–1242
- Freund JB, Vermot J (2014) The wall-stress footprint of blood cells flowing in microvessels. *Biophys J* 106:752–762. <https://doi.org/10.1016/j.bpj.2013.12.020>
- Ghadiri MM, Hosseini SA, Sa S, Rajabpour A (2021) Inertial microfluidics: determining the effect of geometric key parameters on capture efficiency along with a feasibility evaluation for bone marrow cells sorting. *Biomed Microdevice* 23:41. <https://doi.org/10.1007/s10544-021-00577-w>
- Gryczynski Z (2008) FCS imaging—a way to look at cellular processes. *Biophys J* 94:1943–1944
- Hell SW (2007) Far-Field Optical Nanoscopy. *Science* 316:1153–1158. <https://doi.org/10.1126/science.1137395>
- Ho TA, Papavassiliou DV, Lee LL, Striolo A (2011) Liquid water can slip on a hydrophilic surface. *Proc Natl Acad Sci* 108:16170–16175. <https://doi.org/10.1073/pnas.1105189108>
- Hu Z, Zhao T, Wang H et al (2020) Asymmetric temporal variation of oscillating AC electroosmosis with a steady pressure-driven flow. *Exp Fluids* 61:233. <https://doi.org/10.1007/s00348-020-03060-z>
- Hu H, Koochesfahani MM (2006) Molecular tagging velocimetry and thermometry and its application to the wake of a heated circular cylinder. *Meas Sci Technol* 17:1269
- Huang B, Bates M, Zhuang X (2009) Super resolution fluorescence microscopy. *Ann Rev Biochem* 17:993–1016
- Jeyasountharan A, D'Avino G, Giudice FD (2022) Confinement effect on the viscoelastic particle ordering in microfluidic flows: Numerical simulations and experiments. *Phys Fluids* 34:042015. <https://doi.org/10.1063/5.0090997>
- Liu J, Pan Z (2022) Self-ordering and organization of in-line particle chain in a square microchannel. *Phys Fluids* 34:023309. <https://doi.org/10.1063/5.0082577>
- Liu J, Liu H, Pan Z (2021) Numerical investigation on the forming and ordering of staggered particle train in a square microchannel. *Phys Fluids* 33:073301. <https://doi.org/10.1063/5.0054088>
- Jin S, Huang P, Park J, Yoo JY, Breuer KS (2004) Near-surface velocimetry using evanescent wave illumination. *Exp Fluids* 37:825–833
- Joseph P, Tabeling P (2005) Direct measurement of the apparent slip length. *Phys Rev E* 71:035303
- Kim JH, Fiedler HE (1989) Vorticity measurements in a turbulent mixing layer. In: Fernholz H-H, Fiedler HE (eds) *Advances in turbulence 2*. Springer, Berlin Heidelberg, Berlin, Heidelberg, pp 267–271
- Kuang C, Wang G (2010) A novel far-field nanoscopic velocimeter for nanofluidics. *Lab-on-a-Chip* 10:240–245
- Kuang C, Zhao W, Yang F, Wang G (2009) Measuring flow velocity distribution in microchannels using molecular tracers. *Microfluid Nanofluid* 7:509–517
- Kuang C, Qiao R, Wang G (2011) Ultrafast measurement of transient electroosmotic flow in microfluidics. *Microfluid Nanofluid* 11:353–358
- Lauga E, Brenner M, Stone H (2007) Microfluidics: the no-slip boundary condition. In: Tropea C, Yarin AL, Foss JF (eds) *Springer handbook of experimental fluid mechanics*. Springer, Berlin Heidelberg, Berlin, Heidelberg, pp 1219–1240
- Lumma D, Best A, Gansen A, Feuillebois F, Rädler JO, Vinogradova OI (2003) Flow profile near a wall measured by double-focus fluorescence cross-correlation. *Phys Rev E* 67:056313. <https://doi.org/10.1103/PhysRevE.67.056313>
- Martel JM, Toner M (2014) Inertial focusing in microfluidics. *Annu Rev Biomed Eng* 16:371–396. <https://doi.org/10.1146/annurev-bioeng-121813-120704>
- Neto C, Evans DR, Bonaccorso E, Butt HJ, Craig VSJ (2005) Boundary slip in Newtonian liquids: a review of experimental studies. *Rep Prog Phys* 68:2859
- Pittman JL, Henry CS, Gilman SD (2003) Experimental studies of electroosmotic flow dynamics in microfabricated devices during current monitoring experiments. *Anal Chem* 75:361–370. <https://doi.org/10.1021/ac026132n>
- Puyguiraud A, Gouze P, Dentz M (2021) Pore-scale mixing and the evolution of hydrodynamic dispersion in porous media. *Phys Rev Lett* 126:164501. <https://doi.org/10.1103/PhysRevLett.126.164501>
- Rothstein JP (2010) Slip on superhydrophobic surfaces. *Annu Rev Fluid Mech* 42:89–109. <https://doi.org/10.1146/annurev-fluid-121108-145558>
- Santiago JG, Wereley ST, Meinhart CD, Beebe DJ, Adrian RJ (1998) A particle image velocimetry system for microfluidics. *Exp Fluids* 25:316–319
- Schäffel D, Koynov K, Vollmer D, Butt H-J, Schönecker C (2016) Local flow field and slip length of superhydrophobic surfaces. *Phys Rev Lett* 116:134501. <https://doi.org/10.1103/PhysRevLett.116.134501>
- Schembri F, Bodiguel H, Colin A (2015) Velocimetry in microchannels using photobleached molecular tracers: a tool to discriminate solvent velocity in flows of suspensions. *Soft Matter* 11:169–178. <https://doi.org/10.1039/c4sm02049a>
- Schmitz R, Yordanov S, Butt HJ, Koynov K, Dünweg B (2011) Studying flow close to an interface by total internal reflection fluorescence cross-correlation spectroscopy: quantitative data analysis. *Phys Rev E* 84:066306. <https://doi.org/10.1103/PhysRevE.84.066306>
- Sochi T (2011) Slip at fluid-solid interface. *Polym Rev* 51:309–340. <https://doi.org/10.1080/15583724.2011.615961>
- Urschel K, Tauchi M, Achenbach S, Dietel B (2021) Investigation of wall shear stress in cardiovascular research and in clinical practice—from bench to bedside. *Int J Mol Sci* 22:5635
- Vinogradova OI, Koynov K, Best A, Feuillebois F (2009) Direct measurements of hydrophobic slippage using double-focus fluorescence cross-correlation. *Phys Rev Lett* 102:118302. <https://doi.org/10.1103/PhysRevLett.102.118302>
- Wang GR (2005) Laser induced fluorescence photobleaching anemometer for microfluidic devices. *Lab Chip* 5:450–456
- Wang GR, Fiedler HE (2000) On high spatial resolution scalar measurement with LIF. Part 1: photobleaching and thermal blooming. *Exp Fluids* 29:257–264
- Wang GR, Yang F, Zhao W (2014) There can be turbulence in microfluidics at low Reynolds number. *LabChip* 14:1452–1458
- Wang Y, Zhao W, Hu Z et al (2019) Parametric study of the emission spectra and photobleaching time constants of a fluorescent dye in laser induced fluorescence photobleaching anemometer (LIFPA) applications. *Exp Fluids* 60:106. <https://doi.org/10.1007/s00348-019-2751-0>

- Wereley ST, Meinhart CD (2010) Recent advances in micro-particle image velocimetry. *Annu Rev Fluid Mech* 42:557–576. <https://doi.org/10.1146/annurev-fluid-121108-145427>
- Xu M, Yu N, Kim J, Kim C-JC (2021) Superhydrophobic drag reduction in high-speed towing tank. *J Fluid Mech* 908:A6. <https://doi.org/10.1017/jfm.2020.872>
- Zettner ZC, Yoda YM (2003) Particle velocity field measurements in a near-wall flow using evanescent wave illumination. *Exp Fluids* 34:115–121
- Zhao W, Yang F, Khan J, Reifsnider K, Wang G (2016) Measurement of velocity fluctuations in microfluidics with simultaneously ultrahigh spatial and temporal resolution. *Exp Fluids* 56:11. <https://doi.org/10.1007/s00348-015-2106-4>
- Zhao W, Liu X, Yang F et al (2018) Study of oscillating electroosmotic flows with high temporal and spatial resolution. *Anal Chem*. <https://doi.org/10.1021/acs.analchem.7b02985>

Publisher's Note Springer Nature remains neutral with regard to jurisdictional claims in published maps and institutional affiliations.